Tomography of core-mantle boundary and lowermost mantle coupled by geodynamics: joint models of shear and compressional velocity

Gaia Soldati, Lapo Boschi, Steve Della Mora, Alessandro M. Forte

▶ **To cite this version:**

Gaia Soldati, Lapo Boschi, Steve Della Mora, Alessandro M. Forte. Tomography of core-mantle boundary and lowermost mantle coupled by geodynamics: joint models of shear and compressional velocity. Annals of Geophysics, 2014, 57 (6), pp.S0652. 10.4401/ag-6603 . hal-01270758

HAL Id: hal-01270758
https://hal.science/hal-01270758

Submitted on 8 Feb 2016

HAL is a multi-disciplinary open access archive for the deposit and dissemination of scientific research documents, whether they are published or not. The documents may come from teaching and research institutions in France or abroad, or from public or private research centers.

L'archive ouverte pluridisciplinaire **HAL**, est destinée au dépôt et à la diffusion de documents scientifiques de niveau recherche, publiés ou non, émanant des établissements d'enseignement et de recherche français ou étrangers, des laboratoires publics ou privés.

Tomography of core-mantle boundary and lowermost mantle coupled by geodynamics: joint models of shear and compressional velocity

Gaia Soldati[1], Lapo Boschi[2,3], Steve Della Mora[4,5], and Alessandro M. Forte[6]

[1]Istituto Nazionale di Geofisica e Vulcanologia, Roma, Italy.
[2]Sorbonne Universités, UPMC Univ Paris 06, UMR 7193, Institut des Sciences de la Terre Paris (iSTeP), F-75005 Paris, France.
[3]CNRS, UMR 7193, Institut des Sciences de la Terre Paris (iSTeP), F-75005 Paris, France.
[4]Institute of Geophysics, Department of Earth Sciences, ETH Zürich, Switzerland.
[5]Zürich Insurance, Whiteley, U.K.
[6]GEOTOP, Université du Québec à Montréal, Canada

June 11, 2014

Abstract

We conduct joint tomographic inversions of P and S travel time observations to obtain models of δv_P and δv_S in the entire mantle. We adopt a recently published method which takes into account the geodynamic coupling between mantle heterogeneity and core-mantle boundary (CMB) topography by viscous flow, where sensitivity of the seismic travel times to the CMB is accounted for implicitly in the inversion. The approach involved scaling P-wave velocity (more sensitive to the CMB) to density anomalies, in the assumption that mantle heterogeneity has a purely thermal origin, so that velocity and density heterogeneity are proportional to one another. On the other hand, it has sometimes been suggested that S-wave velocity might be more directly sensitive to temperature, while P heterogeneity is more strongly influenced by chemical composition. In the present study, we use only S-, and not P-velocity, to estimate density heterogeneity through linear scaling, and hence the sensitivity of core-reflected P phases to mantle structure. The seismic maps of the Earth's mantle and CMB topography that we derive can explain the inverted seismic data while being physically consistent with each other. Their similarity to the ones obtained by scaling P-velocity to density suggests that compositional anomaly has a limited impact on viscous flow in the deep mantle.

1 Introduction

Our understanding of the dynamics of Earth's mantle is largely based on a precise imaging of its velocity structure. Combining tomographic inversion with geodynamic modelling, and using seismically-inferred density variations as a proxy for CMB topography, *Soldati et al.* (2012) obtained mantle v_P models which are physically sound (their geodynamic coupling to CMB topography is accounted for) and which fit the seismic data (ISC data sets of P-wave arrivals) at least as well as models obtained from seismic data alone. Their method requires that a tomography model of mantle seismic velocity be interpreted in terms of equivalent density anomalies via a constant or radially varying scaling factor. However, density and velocity heterogeneity are proportional to one another only if mantle heterogeneity is of purely thermal origin, and no compositional heterogeneity is present. This is certainly not strictly true, and it is still questioned to what extent it is a valid approximation of the real Earth (e.g. *Karato*, 2003; *Deschamps and Trampert*, 2003; *Trampert et al.*, 2004; *Della Mora et al.*, 2011), at least for the uppermost and lowermost regions of the mantle.

Shear and compressional velocity are in principle sensitive to both composition and temperature, but we do not know a priori the relative importance of the two effects. Since *Soldati et al.* (2012) assume a linear relationship between temperature T and v_P anomalies, we investigate here the other end-member, scaling v_S to T. This is motivated by the stronger sensitivity of S-wave anomalies to temperature (and density) variations (*Goes et al.*, 2000).

We present here a new method to conduct joint inversions of P- and S-waves, which are no longer coupled via any assumption on their scaling; they are now indirectly coupled through the CMB, which is computed by integration of the δv_S heterogeneity structure weighted by the geodynamic sensitivity kernels (*Forte and Peltier*, 1991). This is different from previous joint P-S tomographic models (e.g., *Su and Dziewonski*, 1997; *Vasco and Johnson*, 1998; *Kennett et al.*, 1998; *Saltzer et al.*, 2001; *Kennett and Gorbatov*, 2004; *Houser et al.*, 2008), in that the inversion is now also constrained by the expected physical coupling between mantle and CMB, and no a-priori value for δv_S-to-δv_P scaling is prescribed. Furthermore, only v_S, and not v_P, is attached to density structure, while v_P heterogeneities are completely free parameters. The assumption that δv_S (rather than δv_P) be proportional to density anomaly is motivated by the observation of, e.g., *Boschi et al.* (2007, 2008) that the distribution of deep plume roots correlates much better with lowermost-mantle δv_S than δv_P. We take this as an indication that δv_S is more sensitive than δv_P to thermal variation, while δv_P is more strongly affected by chemical heterogeneity.

The mantle and CMB models we find following this new hybrid approach after scaling v_S velocity to density are almost coincident with the ones obtained by *Soldati et al.* (2012) scaling v_P to density; this is a strong indication that the potential presence of compositional heterogeneity in the lowermost mantle, while it may have important local effects, does not heavily affect the viscous convective flow (*Simmons et al.*, 2009).

2 Method

We assume a linear relationship between travel time data and seismic velocities (*Boschi and Dziewonski*, 2000), and use the LSQR method (*Paige and Saunders*, 1982) to iteratively invert for δv_P and δv_S the following system of equations

$$\delta t_S = -\int_{\text{path}} \frac{\delta v_S(r(s),\theta(s),\phi(s))}{v_S^2(r)} \mathrm{d}s, \tag{1}$$

$$\delta t_P = -\int_{\text{path}} \frac{\delta v_P(r(s),\theta(s),\phi(s))}{v_P^2(r)} \mathrm{d}s, \tag{2}$$

$$\delta t_{PcP} = -\int_{\text{path}} \frac{\delta v_P(r(s),\theta(s),\phi(s))}{v_P^2(r)} \mathrm{d}s + K_{PcP} \frac{\delta c(\theta_b,\phi_b)}{c}, \tag{3}$$

where $r = r(s), \theta = \theta(s), \phi = \phi(s)$ is the ray-path equation, (θ_b, ϕ_b) are the coordinates at which the PcP raypath is reflected off the CMB, and K_{PcP} the sensitivity of δt to CMB undulations (defined e.g. by *Dziewonski and Gilbert* (1976)).

The CMB topography δc is the other unknown function to be determined; *Forte and Peltier* (1991) show that its spherical harmonic coefficients δc_{lm} coincide with the harmonic coefficients $\delta\rho_{lm}$ of density perturbation modulated by the viscosity-dependent CMB sensitivity kernels $B_l(r)$

$$\delta c_{lm} = \frac{1}{\Delta\rho_{cmb}} \int_c^a B_l(r)\delta\rho_{lm}(r)\mathrm{d}r, \tag{4}$$

with c and a denoting the reference, mean radii of the CMB and Earth's surface, respectively, and $\Delta\rho_{cmb}$ the density jump across the CMB according to PREM (*Dziewonski and Anderson*, 1981). The sensitivity kernels B_l are computed adopting the radial viscosity profile selected by *Mitrovica and Forte* (1997) on the basis of the fit to geoid and post-glacial rebound data, neglecting the effect of lateral viscosity variations (*Moucha et al.*, 2007).

Replacing δc in equation 3 with its harmonic expansion 4, and expressing $\delta v_P/v_P$ and $\delta v_S/v_S$ as a linear combination of voxels (*Soldati et al.*, 2012), the system of equations above may be summarized in the compact formula

$$\begin{pmatrix} \delta t_S \\ \delta t_P \\ \delta t_{PcP} \end{pmatrix} = \begin{pmatrix} 0 & A^S_{mantle} \\ A^P_{mantle} & 0 \\ A^{PcP}_{mantle} & A^{PcP}_{CMB} K_{PcP} \end{pmatrix} \cdot \begin{pmatrix} \delta v_P \\ \delta v_S \end{pmatrix}, \tag{5}$$

where the submatrices A^p_{mantle} and A^p_{CMB} represent the sensitivity of the seismic phase p (S, P, PcP) to mantle and CMB structure, respectively. Taking into account the mechanical relationship between deep mantle heterogeneity and CMB deflections allows the equations for δv_P and δv_S to be coupled via the sensitivity kernels K_{PcP}, and the resulting velocity models to be physically consistent with each other and with the CMB topography, obtained from equation 4 after scaling δv_S to $\delta\rho$. Relative density anomalies are indeed assumed to be proportional to shear-velocity ones through the constant factor $\delta ln\rho/\delta lnv_S = 0.27$ (average

of the profile proposed by Karato (1993) on the basis of mineralogical experiments). This simplistic assumption has been proven to be a good approximation of the mineral properties of the mantle through a series of experiments using the depth-dependent scaling factors employed by *Simmons et al.* (2009) and shown in their Figure 3.

We employ a database of ~ 630000 summary rays travel times of P waves and ~ 63000 of PcP waves extracted from the International Seismological Centre (ISC) bulletin, as corrected by *Antolik et al.* (2001), plus the ~ 170000 S waves arrivals computed by Houser et al. (2008) via a cross correlation technique. With respect to our previous study (*Soldati et al.*, 2012), we neglect here the data set of PKP travel times. The combination of the P- and S-wave data sets provides a better coverage throughout most of the mantle and allows us to get a significant increase in information. The velocity models are parametrized in terms of 15 layers (200 km-thick) of 1656 equal area voxels each (plus 1656 pixels to describe the CMB topography), measuring $5^\circ \times 5^\circ$ at the equator.

Multi-parameter inversions may be strongly influenced by factors like the weighting associated with different data or the misfit functions. Following *Soldati et al.* (2012), we assign to each travel time a weight (exponential function) depending on its deviation from PREM predictions. We select different values for the cutoff of our subsets of data, depending on their standard deviation, while we assume the same relative weight for each data set, despite the difference in the number of phase arrivals. The LSQR linearized inversion is regularized via radial and lateral roughness damping only (e.g. *Boschi and Dziewonski*, 1999).

3 Results

3.1 Mantle velocity and CMB topography models

We first compute δv_P and δv_S models of the Earth's mantle and the corresponding CMB topography map via classic tomographic (T) inversions of the entire data set. In this case, the inverse problem 5 is totally decoupled (the geodynamic part of the matrix being null) and therefore equivalent to separate inversions of the *S, P, PcP* data sets. The solution model δv_P, shown in Figure 1 (column 1), is consistent with previously published ones (e.g. *Boschi and Dziewonski*, 1999, 2000; *Soldati et al.*, 2003). The same holds true for the model of mantle δv_S anomalies (column 3), in close agreement with the results found by *Kennett et al.* (1998); *Ritsema et al.* (1999); *Houser et al.* (2008); *Soldati et al.* (2012); *Auer et al.* (2014). Compared to the δv_P solutions, δv_S anomalies are considerably larger and the slow structures

beneath Southern Africa and Pacific Ocean emerge much more clearly; this suggests a stronger sensitivity of v_S to thermal anomalies.

We also show in Figure 1 the results of inverting the entire data set with the tomographic-geodynamic (TG) approach described in Section 2, assuming the radial viscosity profile by *Mitrovica and Forte* (1997). The δv_P and δv_S anomaly maps so obtained (column 2, 4, respectively) are almost coincident with the corresponding T models, derived without considering the mantle-CMB coupling.

As shown in Table 1 , the TG model of δv_P achieves similar or higher variance reduction to the different subsets of data than that associated with the purely tomographic T one, and similarly the TG model of δv_S fits the S data better than the corresponding T model. This is a nontrivial result, since the number of free parameters is reduced in the TG inversion (e.g. *Soldati et al.*, 2012). That a model achieves a higher variance reduction with a lower number of free parameters is an indication that the added regularization provided by geodynamic constraints helps the solution to converge to a better model. The δv_P model of Figure 1 is in agreement with those found by *Soldati et al.* (2012) using the same approach to invert solely the ISC $P-$wave data set, and scaling δv_P (instead of δv_S) to $\delta\rho$ heterogeneity.

We show in Figure 2a our model of CMB topography, obtained directly from the T inversion, and in 2b the model we obtained stepwise from the TG inversion and integration of δv_S as described by *Soldati et al.* (2012). Both models are dominated by harmonic degree 2, corresponding to systematically negative CMB topography under the circumpacific ring. This is generally consistent with the observations of, e.g., *Morelli and Dziewonski* (1987); *Boschi and Dziewonski* (1999); *Rodgers and Wahr* (1993); *Forte et al.* (1995); *Soldati et al.* (2003). With respect to the T model, the TG one is characterized by stronger CMB depression at very high and low latitudes, and an overall smaller amplitude (with a depth-to-valley amplitude of 13.3 km, vs. a value of 14.6 km for the T model).

3.2 Comparison of v_P and v_S models

We show in Figure 3a the correlation between shear and compressional velocity anomalies and that between shear and bulk sound velocity (v_ϕ) anomalies for T and TG mantle models. We observe a positive correlation between δv_P and δv_S throughout the mantle, and a corresponding decorrelation between δv_ϕ and δv_S, with little or no difference between T and TG inversions. All the correlation curves tend to decrease in the midmantle and at D'' depth, as also found by *Della Mora et al.* (2011) inverting direct P and S waves with a clas-

sic tomographic approach and with finer radial parameterization. The simultaneous drop of correlation δv_P-δv_S and anticorrelation δv_ϕ-δv_S at the base of the mantle has been already observed by several studies (e.g. *Su and Dziewonski*, 1997; *Kennett et al.*, 1998; *Becker and Boschi*, 2002; *Antolik et al.*, 2003; *Simmons et al.*, 2010), and may indicate a non-thermal origin for the velocity heterogeneities (*Karato and Karki*, 2001; *Saltzer et al.*, 2001; *Hirose*, 2006).

Another indicator of potential compositional heterogeneity is the ratio $R_{S,P}$ between shear and compressional velocity anomalies, which may be computed following various approaches. Figure 3b shows in red the depth dependence of $R_{S,P}$ computed from Equation 1 of *Della Mora et al.* (2011), while blue and green curves refer to the ratio of the RMS of models δv_S and δv_P, multiplied/not multiplied by the Pearson's correlation coefficient. This coefficient acts as a weight: wherever the correlation between δv_P and δv_S is poor, it is meaningless to assume that they are proportional, and to compute their ratio. Independently from the formula applied, and from the approach used to invert the data (T/TG), $R_{S,P}$ is positive throughout the mantle and increases (of different amounts depending on the formula used to compute it) below 2100 km depth, with a relative maximum around 2600 km depth. This trend is consistent with previous studies (*Saltzer et al.*, 2001; *Della Mora et al.*, 2011), and suggests at least a partial influence of chemical composition on the seismic velocity heterogeneities (*Karato*, 2003). Again, the importance of compositional effects does not appear to be altered by the inclusion of geodynamic constraints (TG) in the inverse problem.

4 Discussion

Using a large data set of P, PcP and S travel time data and the fact that CMB deflections should be gravitationally related to velocity structure of the deep mantle, we apply the method by *Soldati et al.* (2012) to the case of joint inversion for both compressional and shear velocity anomalies. In this approach, CMB topography is not explicitly inverted for, but required to be coupled to mapped mantle heterogeneities according to the viscous flow theory of *Forte and Peltier* (1991). This is a entirely new approach to joint inversion, in that it does not require any assumption on the scaling between v_P and v_S anomalies, which are instead only coupled by the CMB. This study represents a significant extension to that of *Soldati et al.* (2012), in that no scaling was assumed between v_P and density anomalies, but rather between v_S and density anomalies. Interestingly, despite this important difference in

approach, the results of *Soldati et al.* (2012) are confirmed: neither the CMB topography, nor the pattern of mapped low/high velocity are strongly perturbed. The robustness of this result suggests that, while considerable compositional heterogeneity exists in the lowermost mantle, a flow model controlled by temperature/density heterogeneity alone is consistent with the mapped CMB topography and pattern of low/high seismic velocity in the mantle.

Despite the fundamental differences between the results presented here and those of *Soldati et al.* (2012), this is an indication that the global pattern of convective currents in the lower mantle is governed by thermal, rather than thermochemical variations.

References

Antolik, M., G. Ekström, and A. M. Dziewonski (2001), Global event location with full and sparse data sets using three-dimensional models of mantle P-wave velocity, *Pure Appl. Geophysics*, *158*(1-2), 291–317.

Antolik, M., Y. J. Gu, G. Ekström, and A. M. Dziewonski (2003), J362d28: a new joint model of compressional and shear velocity in the Earth's mantle, *Geophysical J. Int.*, *153*(2), 443–466.

Auer, L., L. Boschi, T. W. Becker, T. Nissen-Meyer, and D. Giardini (2014), Savani: A variable-resolution whole-mantle model of anisotropic shear-velocity variations based on multiple datasets, *J. Geophys. Res.*, doi:10.1002/2013JB010773.

Becker, T. W., and L. Boschi (2002), A comparison of tomographic and geodynamic mantle models, *Geochemistry Geophysics Geosystems*, *3*, 10.129/2001GC000,168.

Boschi, L., and A. M. Dziewonski (1999), High- and low-resolution images of the Earth's mantle: Implications of different approaches to tomographic modeling, *J. Geophys. Res.*, *104*(B11), 25,567–25,594.

Boschi, L., and A. M. Dziewonski (2000), Whole Earth tomography from delay times of P, PcP, and PKP phases: Lateral heterogeneities in the outer core or radial anisotropy in the mantle?, *J. Geophys. Res.*, *105*(B6), 13,675–13,696.

Boschi, L., T. W. Becker, and B. Steinberger (2007), Mantle plumes: Dynamic models and seismic images, *Geochemistry Geophysics Geosystems*, *8*, Q10,006, doi:10.1029/2007GC001733.

Boschi, L., T. W. Becker, and B. Steinberger (2008), On the statistical significance of correlations between synthetic mantle plumes and tomographic models, *Phy. Earth. Planet. Int.*, *167*(3-4), 230–238.

Della Mora, S., L. Boschi, P. J. Tackley, T. Nakagawa, and D. Giardini (2011), Low seismic resolution cannot explain S/P velocity decorrelation in the lower mantle, *Geophys. Res. Lett.*, doi:10.1029/2011GL047559.

Deschamps, F., and J. Trampert (2003), Mantle tomography and its relation to temperature and composition, *Phys. Earth Planet. Inter.*, *140*(4), 277–291.

Dziewonski, A. M., and D. L. Anderson (1981), Preliminary reference earth model, *Phy. Earth. Planet. Int.*, *25*(4), 297–356.

Dziewonski, A. M., and F. Gilbert (1976), Effect of small, aspherical perturbations on travel times and a re-examination of corrections for ellipticity, *Geophys. J. Roy. Astron. Soc.*, *44*(1), 7–17.

Forte, A. M., and W. L. Peltier (1991), Viscous-flow models of global geophysical observables 1: Forward problems, *J. Geophys. Res.*, *96*, 20,131–20,159.

Forte, A. M., J. X. Mitrovica, and R. L. Woodward (1995), Seismic-geodynamic determination of the origin of excess ellipticity of the core-mantle boundary, *Geophys. Res. Lett.*, *22*(9), 1013–1016.

Goes, S., R. Govers, and P. Vacher (2000), Shallow mantle temperatures under Europe from P and S wave tomography, *J. Geophys. Res.*, *105*(B5), 11,153–11,169.

Hirose, K. (2006), Postperovskite phase transition and its geophysical implications, *Rev. Geoph.*, *44*.

Houser, C., G. Masters, P. Shearer, and G. Laske (2008), Shear and compressional velocity models of the mantle from cluster analysis of long-period waveforms, *Geophysical J. Int.*, *174*(1), 195–212.

Karato, S. I. (2003), *The dynamic structure of the deep Earth*, Princeton University Press.

Karato, S. I., and B. B. Karki (2001), Origin of lateral variation of seismic wave velocities and density in the deep mantle, *J. Geophys. Res.*, *106*(B10), 21,771–21,783.

Kennett, B., and A. Gorbatov (2004), Seismic heterogeneity in the mantle - strong shear wave signature of slabs from joint tomography, *Phys. Earth Planet. Inter.*, *146*(1-2), 87–100, doi:10.1016/j.pepi.2003.07.033.

Kennett, B. L. N., S. Widiyantoro, and R. D. van der Hilst (1998), Joint seismic tomography for bulk sound and shear wave speed in the Earth's mantle, *J. Geophys. Res.*, *103*(B6), 12,469–12,493.

Mitrovica, J., and A. M. Forte (1997), The radial profile of mantle viscosity: results from the joint inversion of convection and post-glacial rebound observables, *J. Geophys. Res.*, *102*, 2751–2769.

Morelli, A., and A. M. Dziewonski (1987), Topography of the core-mantle boundary and lateral homogeneity of the liquid core, *Nature*, *325*, 678–683.

Moucha, R., A. M. Forte, J. X. Mitrovica, and A. Daradich (2007), Lateral variations in mantle rheology: implications for convection related surface observables and inferred viscosity models, *Geophys. J. Int.*, *169*(1), 113–135.

Paige, C., and M. Saunders (1982), LSQR - an algorithm for sparse linear-equations and sparse least-squares, *ACM Transactions on Mathematical Software*, *8*.

Ritsema, J., H. J. V. Heijst, and J. H. Woodhouse (1999), Complex shear wave velocity structure imaged beneath Africa and iceland, *Science*, *286*(5446), 1925–1928.

Rodgers, A., and J. Wahr (1993), Inference of core-mantle boundary topography from ISC PcP and PKP traveltimes, *Geophys. J. Int.*, *115*, 991–1011.

Saltzer, R. L., R. D. van der Hilst, and H. Karason (2001), Comparing P and S wave heterogeneity in the mantle, *Geophys. Res. Lett.*, *28*(7), 1335–1338.

Simmons, N. A., A. M. Forte, and S. P. Grand (2009), Joint seismic, geodynamic and mineral physical constraints on three-dimensional mantle heterogeneity: Implications for the relative importance of thermal versus compositional heterogeneity, *Geophysical J. Int.*, *177*(3), 1284–1304.

Simmons, N. A., A. M. Forte, L. Boschi, and S. P. Grand (2010), GyPSuM: A joint tomographic model of mantle density and seismic wave speeds., *J. Geophys. Res.*, *115*, B12,310, doi:10.1029/2010JB007,631.

Soldati, G., L. Boschi, and A. Piersanti (2003), Outer core density heterogeneity and the discrepancy between PKP and PcP travel time observations, *Geophys. Res. Lett.*, *30*(4), 1190.

Soldati, G., L. Boschi, and A. Forte (2012), Tomography of core-mantle boundary and lowermost mantle coupled by geodynamics, *Geophys. J. Int.*, doi:10.1111/j.1365-246X.2012.05413.x.

Su, W. J., and A. M. Dziewonski (1997), Simultaneous inversion for 3-D variations in shear and bulk velocity in the mantle, *Phy. Earth. Planet. Int.*, *100*(1-4), 135–156.

Trampert, J., F. Deschamps, J. Resovsky, and D. Yuen (2004), Probabilistic tomography maps chemical heterogeneities throughout the lower mantle, *Science*, *306*(5697), 853–856.

Vasco, D. W., and L. Johnson (1998), Whole earth structure estimated from seismic arrival times, *J. Geophys. Res.*, *103*, 2633–2671.

Mantle/CMB model	S (%)	P (%)	PcP (%)
δv_P (T)	/	25.4	10.2
δv_S (T)	60.3	/	/
δv_P, δv_S (TG)	61.3	25.3	10.5

Table 1: Variance reductions of different databases (columns) achieved by models T and TG, as indicated. Note that model T consists of the results of two entirely decoupled inversions (first and second row), as in *Della Mora et al.* (2011), while model TG (third row) is an individual, joint model including both v_S and v_P anomalies.

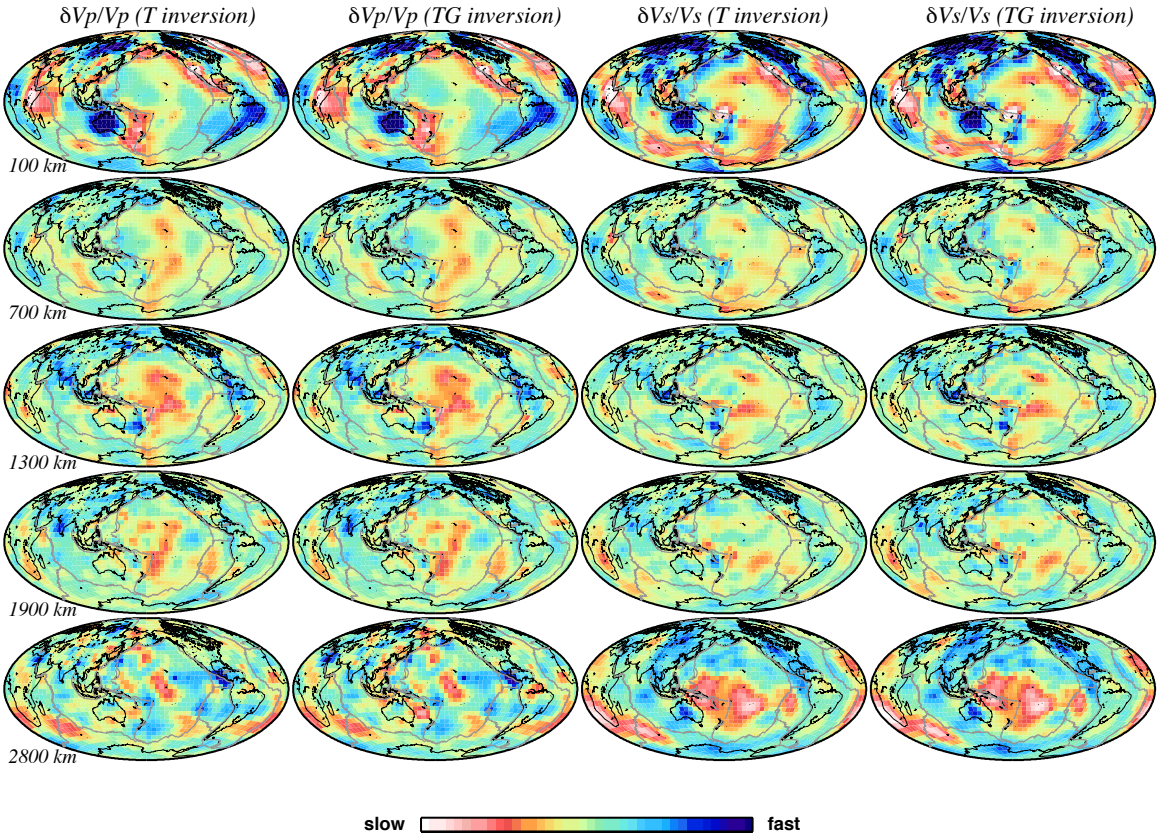

Figure 1: Maps of relative v_P and v_S velocity variations (%) at (top to bottom) five different depths in the mantle, obtained from the entire *P, PcP, S* data set. The maps are derived by jointly inverting ISC and *Houser et al.* (2008) data with a purely tomographic approach T (columns 1, 3), and with a tomographic-geodynamic approach TG (columns 2, 4). The scale for the δv_P maps is $\pm 2\%$ at 100 km depth and $\pm 1\%$ elsewhere, that for the δv_S maps is $\pm 4\%$ at 100 km depth and $\pm 3\%$ elsewhere; blue regions denote higher than average velocity, and red regions denote lower than average velocity.

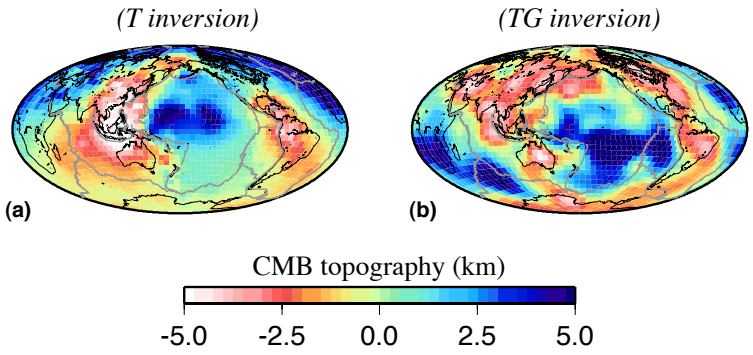

Figure 2: Maps of CMB topography (km) obtained from the entire *P, PcP, S* data set. The maps are obtained by jointly inverting ISC and *Houser et al.* (2008) data with a purely tomographic approach T (a), and with a tomographic-geodynamic approach TG (b), integrating the mantle shear velocity anomaly modulated by the sensitivity kernels as in equation 4.

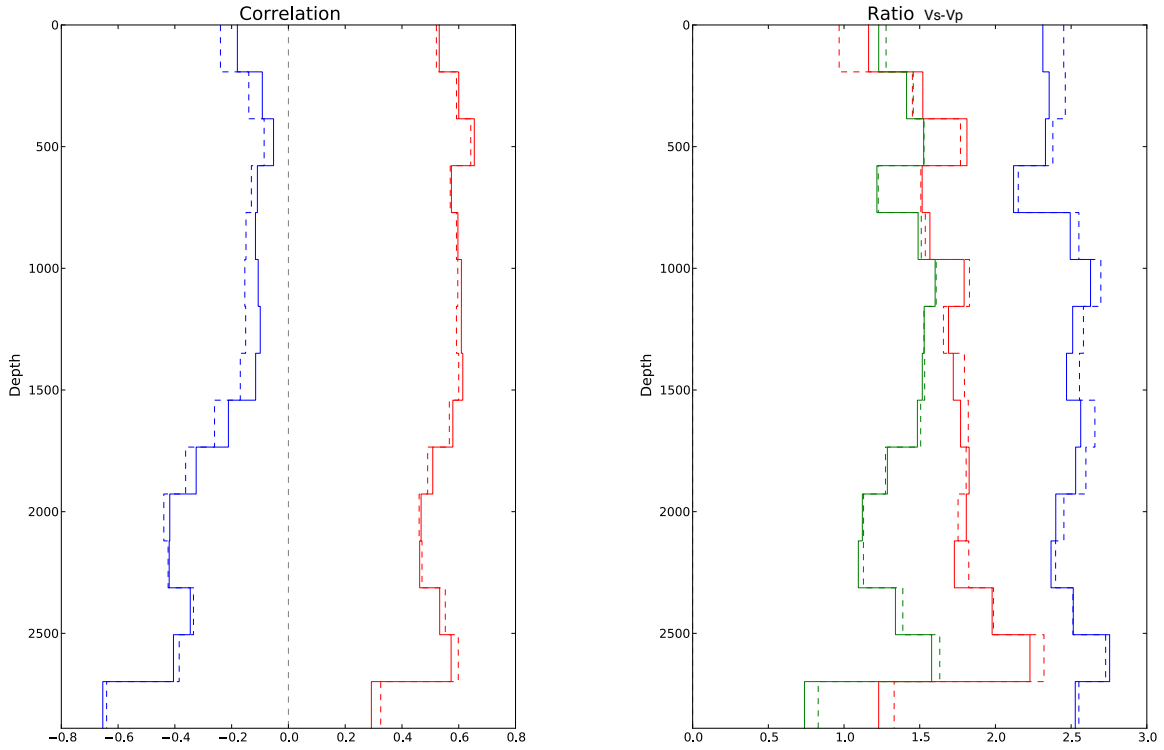

(a) (b)

Figure 3: (a) Radial correlation between v_S and v_P heterogeneities (red) and between bulk sound velocity and v_P heterogeneities (blue), for T (solid) and TG (dashed) mantle models. (b) Ratio between v_S and v_P heterogeneities as a function of depth (red); same ratio computed via the RMS of both models as a function of depth (blue); same as the latter, but multiplied by the v_S-v_P correlation coefficients (panel a, red lines) (green). Solid and dashed lines as in panel a.